JOURNAL OF MATERIALS SCIENCE 16 (1981) 3077–3086

Crystallization-induced superconductivity in amorphous Ti–Ta–Si alloys

A. INOUE, Y. TAKAHASHI,* C. SURYANARAYANA,‡ A. HOSHI, T. MASUMOTO
*The Research Institute for Iron, Steel and Other Metals and * Graduate School, Tohoku University, Sendai 980, Japan*

Amorphous alloys containing 0 to 40 at% Ta and 15 to 20 at% Si have been produced in the ternary Ti–Ta–Si system by rapidly quenching the melts using a melt-spinning technique. The amorphous alloys did not show any superconducting transition down to liquid helium temperature (4.2 K). However, a transition was detected above 4.2 K after inducing crystallization in these alloys by annealing at appropriate temperatures. The superconducting transition temperature, T_c, increased with increasing tantalum content and showed the highest value of 7.6 K for the $Ti_{45}Ta_{40}Si_{15}$ alloy annealed for 1 h at 1073 K. An upper critical magnetic field, H_{c2} of 4.7×10^6 A m^{-1} at 4.2 K and a critical current density, J_c, of 1.5×10^4 A cm^{-2} at zero applied field and 4.2 K were recorded for this alloy. Detailed electron microscopic studies of the crystallization behaviour of the amorphous alloys established that a supersaturated solid solution of tantalum in β-Ti with a bcc structure forms first, followed by the precipitation of the bc tetragonal Ta_3Si compound. Since Ta_3Si is not superconducting above 4.2 K, it has been concluded that superconductivity in the crystallized alloys is due to the precipitation of β-Ti(Ta) solid solution.

1. Introduction

It has been found [1] recently that amorphous superconductors possess high tolerence to irradiation. Thus, amorphous superconductors with a high transition temperature (T_c) as well as good mechanical properties, could be used under high electric/magnetic fields as well as under irradiation conditions. With a view to obtaining an amorphous superconductor with a high T_c and good ductility, we have investigated the composition ranges for the formation of amorphous phases and their superconducting properties in refractory metal (Ti, Zr, Hf, V, Nb, Ta, Mo, W)-based alloys obtained by melt quenching. As a result, we have been successful [2–7] in detecting superconductivity with a T_c above 4.2 K in amorphous alloys of Ti–Nb–(Si, B, C and/or Ge) [2, 3], Nb–(Zr or Mo)–(Si, B, C and/or Ge) [4, 5] and (Mo or W)–Si–B [6, 7] systems. Very recently, we also found a ductile amorphous single phase with complete bend ductility in the Ti–Ta–Si system. The formation range is quite similar to that for the Ti–Nb–Si [2] and Ti–V–Si [8] amorphous alloys. Additionally, it was expected that the Ta_3Si compound with the A-15 cubic structure possessing a high T_c and upper critical magnetic field, H_{c2}, may precipitate in the Ti–Ta–Si alloys crystallized from the amorphous state. The present paper describes the composition range for the formation of the amorphous phase in the Ti–Ta–Si system, the crystallization behaviour of the amorphous phase and the superconducting properties of the crystallized alloys.

2. Experimental details

Mixtures of 99.5 wt% pure titanium, 99.9 wt% pure tantalum and 99.999 wt% pure silicon were melted in an arc furnace on a water-cooled copper

‡Present address: Department of Metallurgical Engineering, Banaras Hindu University, Varanasi 221005, India.

0022–2461/81/113077–10$03.00/0 © *1981 Chapman and Hall Ltd.*

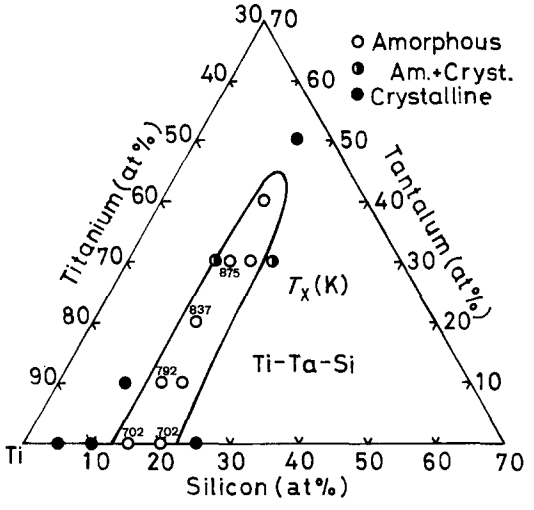

Figure 1 Composition range for formation of an amorphous phase in the Ti–Ta–Si system.

hearth with a non-consumable tungsten electrode. Melting was accomplished in a purified and gettered argon atmosphere at a pressure of about 8×10^4 Pa. The compositions of the alloys reported are the nominal ones since the losses during melting were negligible.

The method of producing ribbon specimens of about 1 mm width and 0.02 mm thickness and methods of characterizing them by X-ray and electron metallographic techniques have previously been described [8]. The crystallization temperatures were determined using a differential thermal analyser (DTA) while continuously heating the alloys at a constant rate of 8.33×10^{-2} K sec^{-1}. The Vickers hardness was measured with a 100 g load and ductility was evaluated by a simple bend test. Methods for evaluating the superconducting properties have been described by Inoue *et al.* [2].

3. Results

3.1. Formation range of the amorphous phase

The composition of the melt-quenched Ti–Ta–Si ternary alloys at room temperature is shown in Fig. 1 which maps the amorphous and crystalline phase fields. It can be seen that the amorphous phase forms in the wide composition ranges 0 to 40 at% Ta and 15 to 20 at% Si. The amorphous nature of these alloys has been confirmed by electron microscopy and electron diffraction. Fig. 2 shows a bright-field electron micrograph and the corresponding diffraction pattern for a thinned $Ti_{65}Ta_{20}Si_{15}$ alloy. The lack of features in (a) and the diffuse haloes in (b) confirm the amorphous nature of this phase.

According to Turnbull [9], a deep eutectic in an alloy system is connected with a comparatively large negative heat-of-formation. It is also observed that many amorphous phases have been detected in alloys corresponding to the eutectic compositions [10]. The binary systems Ti–Si [11] and Ta–Si [12] feature eutectic reactions at 14 at% Si and 1606 K, and 15 at% Si and 2580 K, respectively. An amorphous phase has already been reported near the eutectic composition in Ti–Si alloys [13]. Thus, the present amorphous-phase forming composition range also falls near the trough of the eutectic in the Ti–Ta–Si ternary system, indicating that the ease of formation of an amorphous phase is closely related to the large negative heat-of-formation of the liquid alloy.

3.2. Mechanical properties and crystallization temperature

Vickers hardness (H_v), tensile fracture strength (σ_f), crystallization temperature (T_x) and the

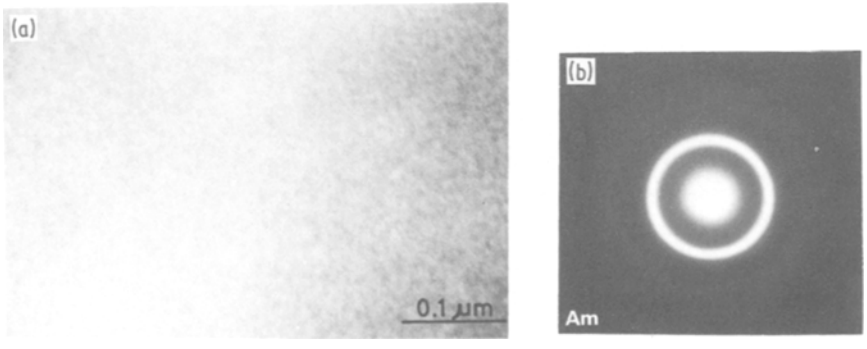

Figure 2 (a) Transmission electron micrograph and (b) selected-area diffraction pattern showing the as-quenched structure of $Ti_{65}Ta_{20}Si_{15}$ alloys.

TABLE I Vickers hardnesses (H_v), tensile fracture strength (σ_f), crystallization temperature (T_x) and critical fracture temperature (T_f) for several Ti–Ta–Si amorphous alloys

Alloy system (at%)	Vickers hardness, H_v (DPN)	Tensile fracture strength, σ_f (MPa)	Crystallization temperature T_x(K), 8.33×10^{-2} K sec^{-1}	Critical fracture temperature T_f (K), 3600 sec
$Ti_{75}Ta_{10}Si_{15}$	595	2220	792	–
$Ti_{72}Ta_{10}Si_{18}$	610	–	816	–
$Ti_{65}Ta_{20}Si_{15}$	620	2230	837	750
$Ti_{55}Ta_{30}Si_{15}$	640	2280	875	680
$Ti_{52}Ta_{30}Si_{18}$	640	–	877	–
$Ti_{45}Ta_{40}Si_{15}$	680	2390	910	660

critical fracture temperature (T_f) of $Ti_{85-x}Ta_xSi_{15}$ amorphous alloys are shown in Table I. Here T_f is the temperature of ageing for 3600 sec which led to the fracture of alloys in a simple bend test. The hardness and the tensile strength values are in the range 600 to 680 DPN* and 2200 to 2400 MPa, respectively. The crystallization and critical fracture temperatures are in the range 790 to 910 K and 680 to 750 K, respectively. One can see that H_v, σ_f and T_x increase with increasing tantalum content while T_f shows the oppisite trend. No clear trend in the properties with silicon content is recognized.

These amorphous alloys posses very good bend ductility. Fig. 3 shows the deformation structure of a $Ti_{45}Ta_{40}Si_{15}$ amorphous alloy bent completely over the edge of a thin razor blade. While numerous deformation markings can be seen near the bent edge, no cracks are observed.

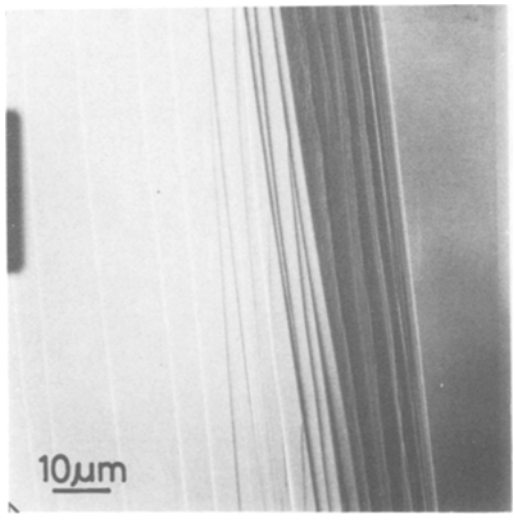

Figure 3 Scanning electron micrograph showing the deformation markings at the tip of $Ti_{45}Ta_{40}Si_{15}$ amorphous alloy bent through 180°.

* Diamond pyramid number.

3.3. Crystallization behaviour

Fig. 4 shows the DTA curve for the $Ti_{75}Ta_{10}Si_{15}$ alloy. Similar behaviour has been observed in other alloys also. The curve exhibits two exothermic peaks suggesting that crystallization might take place in two stages. To obtain a better understanding of the crystallization behaviour and the nature of the phases produced, detailed transmission electron microscopic observations have been carried out and representative results are shown in Fig. 5.

On ageing for 1800 sec at 773 K, fine precipitates (mostly with a rectangular cross-section) are seen over the entire specimen area (Fig. 5a). These crystals have a very slow growth rate and average size of less than 25 nm. The corresponding diffraction pattern, Fig. 5b, clearly shows that both the amorphous phase and the crystalline phase with a bcc structure co-exists. Thus, it has been shown that these fine particles have a bcc structure with a lattice parameter of $a \simeq 0.33$ nm, which corresponds to a β-Ti(Ta) solid solution [14]. No other crystalline phase could be detected at this

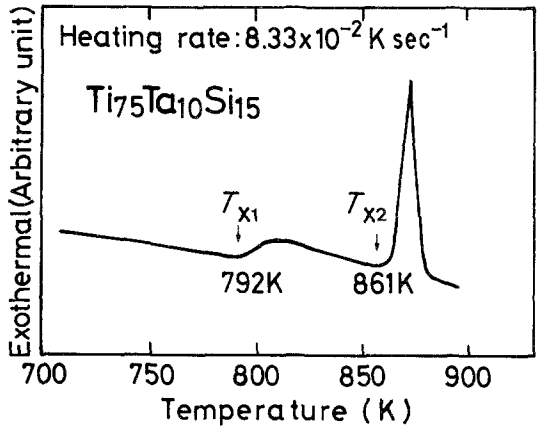

Figure 4 Differential thermal analysis curve of $Ti_{75}Ta_{10}Si_{15}$ amorphous alloy.

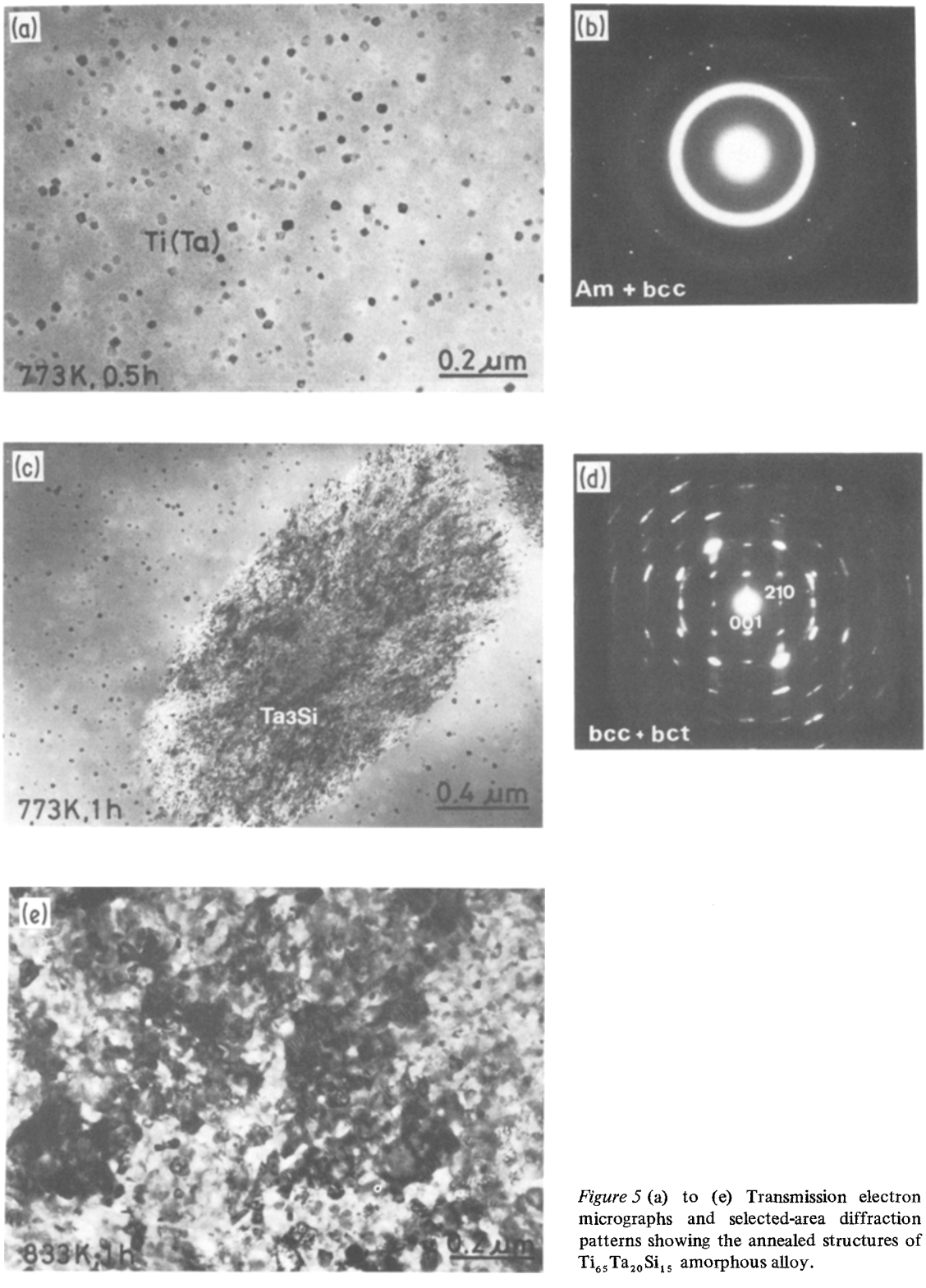

Figure 5 (a) to (e) Transmission electron micrographs and selected-area diffraction patterns showing the annealed structures of $Ti_{65}Ta_{20}Si_{15}$ amorphous alloy.

stage of decomposition. Since the β-Ti(Ta) solid solution is stable only at higher temperatures and not at room temperature, the β-Ti(Ta) solid solution present at room temperature can be considered metastable. According to the terminology used in the literature, we can call this MS-I, a supersaturated solid solution of tantalum in β-Ti. The very slow growth of MS-I particles may be due to the enrichment of silicon in the amorphous phase.

Ageing for 3600 sec at 773 K results in the precipitation of a second crystalline phase, MS-II, coexisting with MS-I. MS-II phase particles are large and have an oval shape (Fig. 5c). The electron diffraction pattern recorded from the MS-II particles (Fig. 5d) clearly shows that they are Ta_3Si with a bc tetragonal structure with $a \simeq 1.02$ nm and $c \simeq 0.52$ nm. Another interesting feature of the MS-II particles is that they contain a large number of internal defects which could have resulted from the internal strain generated during crystallization. Ta_3Si particles have an average size of about 1 μm diameter and 2 μm length and are much larger than the MS-I particles.

At higher annealing temperatures, the remaining amorphous phase completely transforms to a mixture of β-Ti(Ta) and Ta_3Si phases (Fig. 5e) and eventually to α-Ti + Ta_3Si. At no temperature was the Ta_3Si phase with the cubic A-15 structure detected in the present investigation (Fig. 6). The detailed crystallization behaviour is represented in Table II.

From the foregoing it can be concluded that the first peak in the DTA curve (broad and low intensity) corresponds to the precipitation of β-Ti(Ta) while the second (narrow and high intensity) peak corresponds to the precipitation of the Ta_3Si compound. Thus, the crystallization sequence in these alloys can be represented as:

$$\text{Am} \rightarrow \text{Am}' + \text{MS-I} \rightarrow \text{MS-I} + \text{MS-II} \rightarrow \text{Stable phases.}$$

Such a sequence agrees with that in other Ti-based amorphous alloys [8, 13, 15, 16].

3.4. Superconducting properties

Electrical resistance in the vicinity of T_c was measured for the $Ti_{85-x}Ta_xSi_{15}$ alloys both in the as-quenched and annealed conditions under no applied magnetic field. The annealing treatment was carried out for 3600 sec at temperatures ranging from 923 to 1173 K. The value of T_c was taken as the temperarure corresponding to $R/R_n = 0.5$, where R_n is the resistance in the normal state. The transition width ΔT_c is the temperature difference between 0.1 and 0.9 of R/R_n. The values of T_c and ΔT_c are plotted in Fig. 7 as a function of the annealing temperature. The amorphous alloys continued to exhibit normal state resistance down to liquid helium temperature. This result is similar to that noted for amorphous Ti–V–Si alloys [8], but different from that of Ti–Nb–Si alloys [2], which show superconductivity in the amorphous state. A possible reason for this anomalous behaviour could be the relatively low T_c values (4.48 and 5.30 K) of tantalum and vanadium compared to the high value (9.23 K) of niobium. The crystallized Ti–Ta–Si alloys, however, show a very clear and complete superconducting transition similar to the Ti–Nb–Si [15] or Ti–V–Si [8] alloys. Fig. 7 shows that T_c increases with increasing tantalum content. Another observation that can be made is that T_c increases with annealing temperature, reaches a peak value and then decreases with further heating. The highest T_c values attained are 6.9 K for $Ti_{65}Ta_{20}Si_{15}$, 7.3 K for $Ti_{55}Ta_{30}Si_{15}$ and 7.6 K for $Ti_{45}Ta_{40}Si_{15}$.

The critical current density (J_c) was measured by a standard four-probe resistance method at external applied magnetic field (H) in a liquid helium bath. As an example, we chose the $Ti_{45}Ta_{40}Si_{15}$ alloy which showed the highest T_c. $J_c(H)$ as a function of H for this alloy annealed for 1 h at various temperatures is shown in Fig. 8. For $H = 0$, J_c is about 1.5×10^4 A cm^{-2} and decreases rapidly with increasing H when the alloy is annealed at 923 K. On the other hand, J_c remains fairly constant up to a H value of about 3.5×10^6 A m^{-1} for the specimens annealed at temperatures ranging from 973 to 1173 K. At higher field values, J_c drops sharply for all the alloys. Thus, the flux pinning force (given by the area under the J_c–H curve) shows a maximum value for anneals at 1023 K for the $Ti_{45}Ta_{40}Si_{15}$ alloy. This is found to be true in the case of other alloys also. Further, one can see that the upper critical magnetic field (H_{c2}) is about 4.7×10^6 A m^{-1} when the alloy is annealed at 1023 K. Here, we define H_{c2} as the applied magnetic field at which the resistance of the sample reaches half its normal value.

4. Discussion

4.1. Change in T_c with alloy composition and annealing temperature

The present transmission electron microscopic

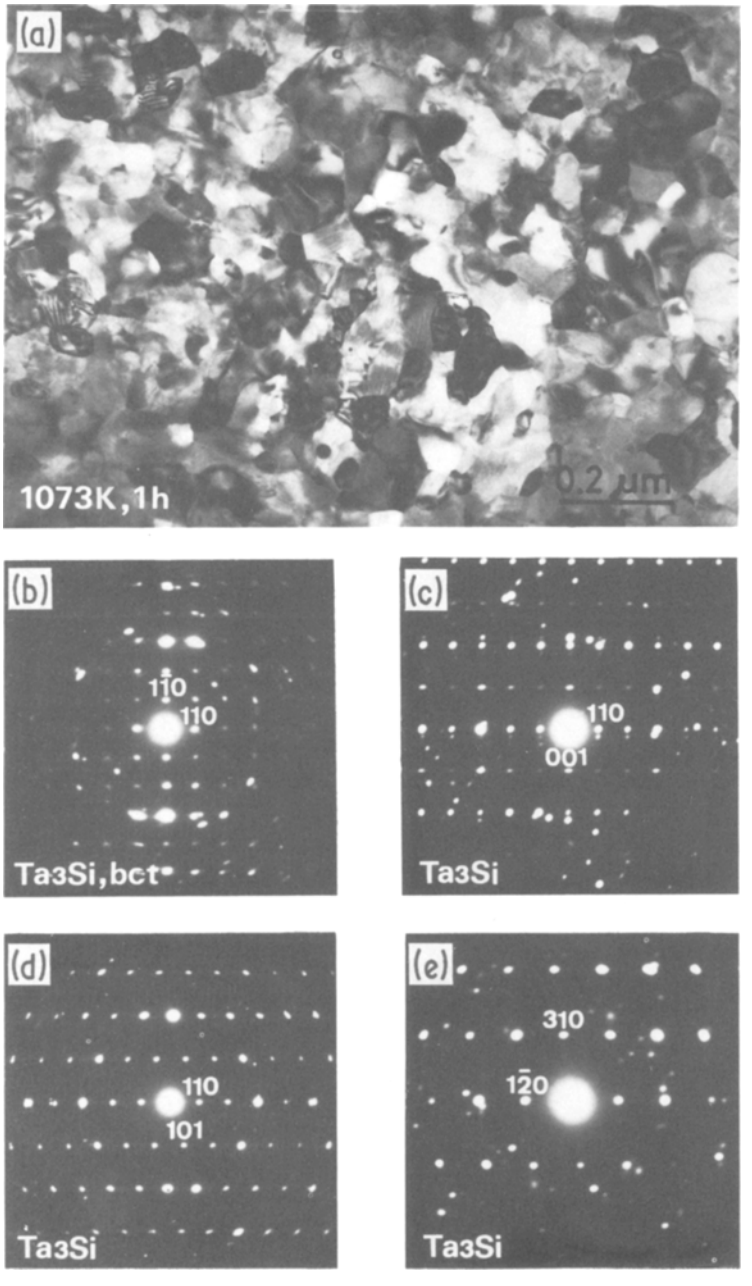

Figure 6 (a) Transmission electron micrograph and (b) to (e) selected diffraction patterns of $Ti_{65}Ta_{20}Si_{15}$ amorphous alloy annealed for 1 h at 1075 K.

observations have indicated that the specimens showing the highest T_c consist of the bcc β-Ti(Ta) solid solution and the bc tetragonal Ta_3Si compound. Deardorff *et al.* [17] reported that the bct Ta_3Si compound is non-superconducting above 4.2 K. Hence, it is concluded that superconductivity in crystallized Ti–Ta–Si alloys is due to the precipitation of the β-Ti(Ta) solid solution, similar to the mechanism for the superconducting binary Ti–Ta alloys [18]. It has been well recognized that T_c is independent of the microstructural features, e.g. in this case, the grain size of the β-Ti(Ta) solid solution or size of the Ta_3Si particles. Thus, the marked change in T_c on annealing can be correlated with a change in the tantalum content of the solid solution. The decrease in T_c beyond the peak value may be attributed to the formation of the equilibrium α-Ti (hcp) phase from the metastable β-Ti (bcc) phase. Earlier investigations of Colling *et al.* [18] showed that the T_c of crystalline Ti–Ta binary alloys changes with tantalum content. For example,

TABLE II Crystallization process of Ti_{85-x}(V, Nb or Ta)$_x Si_{15}$ amorphous alloys

(1) $Ti_{45-65}Ta_{20-40}Si_{15}$

Am. → Am. + β-Ti(Ta) → β-Ti(Ta) + Ta_3Si + (ω) → β-Ti(Ta) + Ta_3Si + (α-Ti)

β-Ti(Ta) : bcc, $a \simeq 0.33$ nm

Ta_3Si : bc tetragonal, $a \simeq 1.02$ nm, $c \simeq 0.52$ nm

ω : hexagonal, $a \simeq 0.46$ nm, $c \simeq 0.28$ nm

α-Ti : hcp, $a \simeq 0.295$ nm, $c \simeq 0.468$ nm

(2) $Ti_{55-80}V_{5-30}Si_{15}$

Am. → Am. + β-Ti(V) → β-Ti(V) + hexagonal Ti_5Si_3 + (ω) → β-Ti(V) + Ti_5Si_3 + (α-Ti)

(3) $Ti_{45-75}Nb_{10-40}Si_{15}$

Am. → Am. + β-Ti(Nb) → β-Ti(Nb) + bc tetragonal Nb_3Si + (ω) → β-Ti(Nb) + Nb_3Si + (α-Ti)

it was reported that T_c is about 4.8 K for $Ti_{80}Ta_{20}$ and that it increases gradually with tantalum content, reaching a value of 8.9 K for $Ti_{50}Ta_{50}$. The tantalum content in the $Ti_{65}Ta_{20}Si_{15}$ alloy corresponds to about 23.5 at% for the pseudobinary Ti–Ta alloy and the T_c for $Ti_{76.5}Ta_{23.5}$ is estimated to be 5.4 K from the previous data [18]. However, as seen from Fig. 7, the $Ti_{65}Ta_{20}Si_{15}$ alloy shows T_c values higher than 5.4 K in the temperature range 973 to 1123 K and the highest T_c recorded is about 6.9 K at 1073 K. This value corresponds to the binary crystalline $Ti_{71}Ta_{29}$, indicating that the high T_c in these alloys is due to the enrichment of tantalum in the β-phase. On the other hand, the highest T_c values (7.3 and 7.6 K) of $Ti_{55}Ta_{30}Si_{15}$ and $Ti_{45}Ta_{40}Si_{15}$ alloys are lower than those (7.7 and 8.6 K) of the pseudobinary $Ti_{65}Ta_{35}$ and $Ti_{53}Ta_{47}$ alloys. This difference is found to increase with increasing tantalum content. Such a lowering in T_c for the Ti–Ta–Si alloys containing large amounts of tantalum appears to be related to the crystallization behaviour as follows: The Ta_3Si compound precipitates out immediately after the β-phase begins to appear and hence the tantalum content in the β-phase is not high. This inference receives support from the result that with increasing tantalum content, the broad DTA peak (corresponding to the precipitation of the β-phase) shifts to higher temperatures and the sharp peak (corresponding to the precipitation of the Ta_3Si compound) hardly

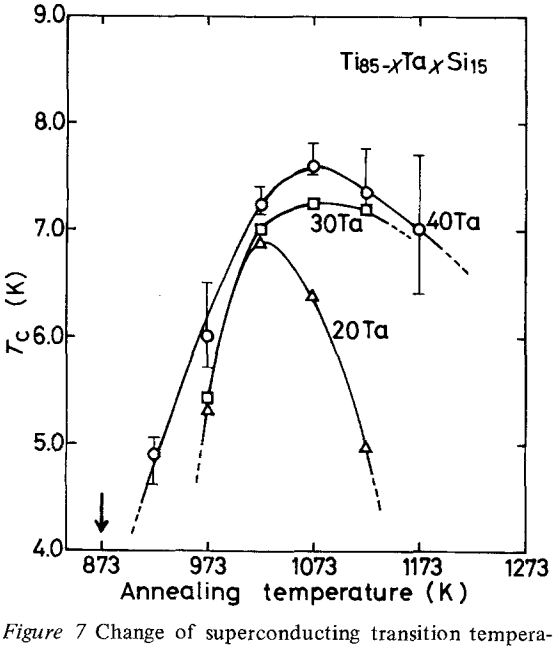

Figure 7 Change of superconducting transition temperature T_c for $Ti_{85-x}Ta_xSi_{15}$ amorphous alloys with annealing temperature. The vertical bars correspond to ΔT_c.

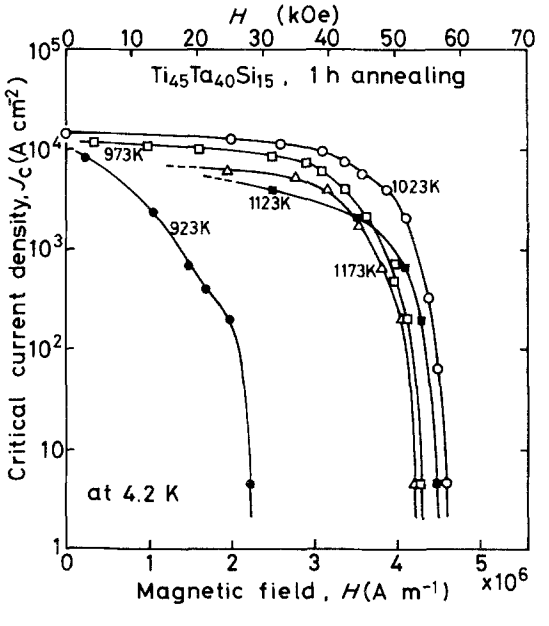

Figure 8 Critical current density (J_c) of $Ti_{45}Ta_{40}Si_{15}$ amorphous alloy annealed for 1 h at various temperatures as a function of magnetic field applied normal to the direction of current flow.

changes. Another observation that supports this hypothesis is that the annealing temperature required for the highest T_c increases with increasing tantalum content, which again is due to the higher T_x values for the precipitation of the β-phase in higher tantalum content alloys.

As already indicated, the transition temperature decreases rapidly after reaching the peak value. This trend is more pronounced in alloys containing a small amount of tantalum. The reason for this decrease may be the formation of the α-Ti phase. As shown in Table II, the β-Ti(Ta) solid solution transforms to the α-Ti phase after the formation of the Ta_3Si compound. This transformation is facilitated by the precipitation of the Ta_3Si compound since a large amount of tantalum is required for the formation of Ta_3Si and thus the β-matrix is depleted of tantalum. Since the solid solubility of tantalum in α-Ti is much less than that in β-Ti [11], the tantalum-depleted β-phase can transform to α-Ti. Thus, the lowering of T_c beyond the peak is both due to a decrease in the tantalum content of the β-solid solution and formation of α from the β-phase. The volume-fraction of α-phase decreases with increasing tantalum content and hence the tendency for lowering of T_c becomes weak as seen in Fig. 7.

4.2. Comparison of crystallization behaviour and the resultant superconducting properties among amorphous Ti–(V, Nb or Ta)–Si alloys

The crystallization processes of Ti_{85-x}(V, Nb or Ta)$_xSi_{15}$ amorphous alloys, clarified by the present authors [8, 15], are summarized in Table II. These alloys transform to the stable phases through the formation of MS-I and MS-II phases. The MS-I phase is a β-Ti(V, Nb or Ta) solid solution for the three-alloy system, the MS-II phase is the b c tetragonal (Nb or Ta)$_3$Si for the Ti–Nb–Si and Ti–Ta–Si systems, and the hexagonal Ti_5Si_3 for the Ti–V–Si system. Thus, a V_3Si-type compound was not detected in the Ti–V–Si system. This result suggests that the bonding between titanium, vanadium, niobium or tantalum and silicon becomes progressively weaker in the order of $Ta_3Si \simeq Nb_3Si > Ti_5Si_3 > V_3Si$ and the forming tendency of A-15-type cubic compounds such as V_3Si, Nb_3Si and Ta_3Si is weaker than that of b c tetragonal (Nb or Ta)$_3$Si or hexagonal Ti_5Si_3 compounds.

The highest T_c values of Ti_{85-x}(V, Nb or Ta)$_x$ Si_{15} alloys annealed for 3600 sec at various temperatures from the amorphous state are plotted as a function of vanadium, niobium or tantalum concentration in Fig. 9, based on the previous [8, 15] and present results. T_c shows peak values for the alloys containing about 30 to 40 at% V, Nb or Ta and the T_c of Ti–Nb–Si alloys is much higher than that of Ti–V–Si and Ti–Ta–Si alloys. Further, the alloy concentration at which a superconducting transition begins to appear (at temperatures above 4.2 K) shifts to the high concentration side in the order: vanadium, niobium and tantalum. It is remarkable that the alloy containing as little as 5 at% V exhibits a $T_c \simeq 5.0$ K. This is closely related to the fact [11] that the alloy composition where the $\beta \rightarrow \alpha$ transformation occurs in each binary alloy system is located on the high concentration side in the order: vanadium, niobium and tantalum. That is, for the Ti–V–Si alloys the β-phase is stable even at very low vanadium compositions and hence the $\beta \rightarrow \alpha$ transformation is suppressed. In addition, the MS-II phase in Ti–V–Si alloys is Ti_5Si_3 and hence a large amount of vanadium dissolves in the β-phase, leading to its greater stability. This may be the reason why the Ti–V–Si alloys exhibit a high T_c even at low vanadium concentrations.

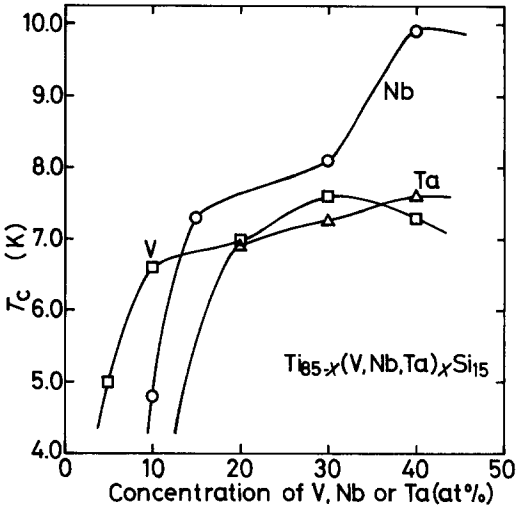

Figure 9 Change of maximum superconducting transition temperature (T_c) for Ti_{85-x}(V, Nb or Ta)$_xSi_{15}$ alloys crystallized from the amorphous state with concentration of vanadium, niobium or tantalum.

Fig. 10 shows the H_{c2} of Ti_{85-x}(V, Nb or Ta)$_x$ Si_{15} alloys as a function of annealing temperature. The H_{c2} value increases in the order of tantalum, vanadium and niobium and it is to be noticed

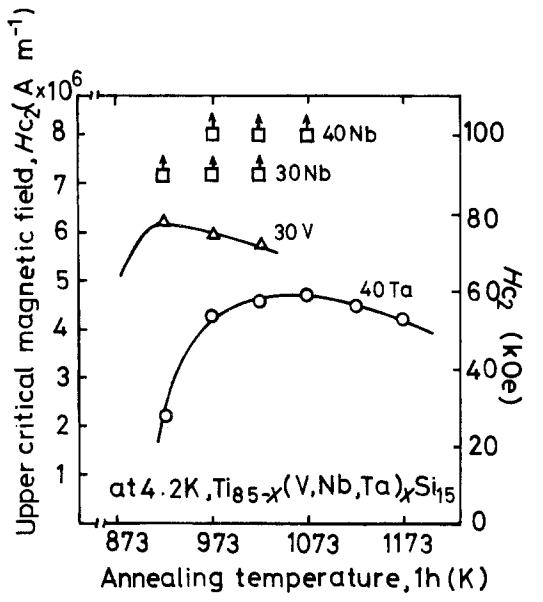

Figure 10 Change of upper critical magnetic field (H_{c_2}) for Ti_{85-x}(V, Nb or Ta)$_x$Si$_{15}$ amorphous alloys with annealing temperature.

that the $Ti_{45-55}Nb_{30-40}Si_{15}$ alloys exhibit H_{c2} values higher than 9 to 10 tesla in the wide range of annealing temperatures. It is evident from the above-described results that the most appropriate alloy system for endowing good superconductivity via crystallization from the amorphous state is the Ti–Nb–Si system and the highest T_c, H_{c2} and J_c are about 10 K, above 10 tesla, and about 10^5 A cm^{-2}, respectively. These values are almost equivalent to those [19] of conventional Ti–Nb binary alloys. Therefore, from the technological point of view, the present results seem to suggest the possibility that the melt-quenching technique makes the processing of superconducting materials much simpler. First, the amorphous ribbons which are very flexible can be fabricated by the now well-developed techniques of melt-spinning, used in the proper assembly for application and then heat-treated to produce the desired superconducting properties.

5. Conclusions

Amorphous alloys possessing high strength and good bend ductility were found in a wide composition range in the Ti–Ta–Si system. Continuous ribbons of about 1 mm width and about 0.02 mm thickness were produced using a melt-spinning apparatus designed for high melting alloys. The amorphous phase could be obtained in alloys containing 0 to 40 at% Ta and 15 to 20 at% Si. Vickers hardness and tensile strength were about 630 DPN and 2280 MPa, respectively. Crystallization temperatures were in the range 790 to 910 K. Further, these amorphous alloys were so ductile that no crack was found at the tip of a specimen bent through 180°. The specimens continued to be ductile when annealed for 1 h at temperatures below about 660 K.

The Ti–Ta–Si amorphous alloys were not superconducting, but showed a superconducting transition above the liquid helium temperature (4.2 K) after crystallization. The transition temperature, T_c, increased with increasing tantalum content and reached a value as high as 7.6 K for $Ti_{45}Ta_{40}Si_{15}$. The same tendency was recognized for the upper critical magnetic field, H_{c2}, and the critical current density, J_c. The values of H_{c2} and J_c obtained were of the order of 4.7×10^6 A m^{-1} at 4.2 K and 1.5×10^4 A cm^{-2} at zero applied field and 4.2 K for $Ti_{45}Ta_{40}Si_{15}$ alloy. The structure of the superconducting samples consisted of bcc β-Ti(Ta) and bc tetragonal Ta_3Si phases. Since Ta_3Si is not superconducting above 4.2 K, it was concluded that superconductivity in these alloys resulted from the precipitation of the β-phase, a supersaturated solid solution containing much more tantalum than the equilibrium limit.

Acknowledgements

The authors are indebted to Messrs. M. Kudo, K. Sai and Y. Ishikawa of the High Magnetic Field Laboratory of Tohoku University for critical magnetic field measurements. CS is grateful to the Japanese Society for the Promotion of Science for financial assistance.

References

1. E. A. KRAMER, W. L. JOHNSON and C. CLINE, *Appl. Phys. Lett.* **35** (1979) 815.
2. A. INOUE, H. KIMURA, T. MASUMOTO, C. SURYANARAYANA and A. HOSHI, *J. Appl. Phys.* **51** (1980) 5475.
3. A. INOUE, T. MASUMOTO, C. SURYANARAYANA and A. HOSHI, *J. de Physique* **41** (1980) C8–758.
4. T. MASUMOTO, A. INOUE, S. SAKAI, H. M. KIMURA and A. HOSHI, *Trans. Japan Inst. Met.* **21** (1980) 115.
5. A. INOUE, T. MASUMOTO, A. HOSHI and S. SAKAI, Conference on Metallic Glasses, Science and Technology, Budapest, Hungary, June/July, 1980.
6. A. INOUE, S. SAKAI, H. M. KIMURA, T. MASUMOTO and A. HOSHI, *Scripta Met.* **14** (1980) 235.
7. A. INOUE, Y. TAKAHASHI, K. AOKI, S. SAKAI and T. MASUMOTO, to be presented at the 4th

International Conference on Rapidly Quenched Metals, Sendai, Japan, August 1981.
8. A. INOUE, C. SURYANARAYANA, T. MASUMOTO and A. HOSHI, *Mater. Sci. Eng.* **44** (1981) 69.
9. D. TURNBULL, *J. Phys. (Paris) Colloq.* **35** (1974) 1.
10. C. SURYANARAYANA, "Rapidly Quenched Metals –A Bibliography 1973–1979", (IFI Plenum, New York, 1980).
11. C. J. SMITHELLS, "Metals Reference Book", 5th edn. (Butterworths, London, 1976) p. 782.
12. "Metals Handbook, Metallography, Structures and Phase Diagrams", 8th edn. (American Society for Metals, Metals Park, Ohio, 1973) p. 334.
13. C. SURYANARAYANA, A. INOUE and T. MASUMOTO, *J. Mater. Sci.* **15** (1980) 1993.
14. W. B. PEARSON, "A Handbook of Lattice Spacings and Structures of Metals and Alloys", (Pergamon Press, Oxford, 1967) p. 867.
15. A. INOUE, C. SURYANARAYANA, T. MASUMOTO and A. HOSHI, *Sci. Rep. Res. Inst. Tohoku Univ.* **A-28** (1980) 182.
16. C. SURYANARAYANA, A. INOUE and T. MASUMOTO, *ibid.* **A-28** (1980) 195.
17. D. K. DEARDORFF, R. E. SIEMENS, P. A. ROMANS and R. A. MCCUNE, *J. Less-Common Metals* **18** (1969) 11.
18. D. A. COLLING, K. M. RALLS and J. WULFF, *J. Appl. Phys.* **37** (1966) 4570.
19. Y. AIYAMA, "Superconductivity" (The Physics Society of Japan, Maruzen, Tokyo, 1979) p. 265.

Received 27 February and accepted 9 April 1981.